Development 136, 2039-2048 (2009) doi:10.1242/dev.030601

PTK7 is essential for polarized cell motility and convergent extension during mouse gastrulation

Wei Wei Yen[1], Margot Williams[1], Ammasi Periasamy[2,3], Mark Conaway[4], Carol Burdsal[5], Raymond Keller[2], Xiaowei Lu[1] and Ann Sutherland[1,*]

Despite being implicated as a mechanism driving gastrulation and body axis elongation in mouse embryos, the cellular mechanisms underlying mammalian convergent extension (CE) are unknown. Here we show, with high-resolution time-lapse imaging of living mouse embryos, that mesodermal CE occurs by mediolateral cell intercalation, driven by mediolaterally polarized cell behavior. The initial events in the onset of CE are mediolateral elongation, alignment and orientation of mesoderm cells as they exit the primitive streak. This cell shape change occurs prior to, and is required for, the subsequent onset of mediolaterally polarized protrusive activity. In embryos mutant for PTK7, a novel cell polarity protein, the normal cell elongation and alignment upon leaving the primitive streak, the subsequent polarized protrusive activity, and CE and axial elongation all failed. The mesoderm normally thickens and extends, but on failure of convergence movements in *Ptk7* mutants, the mesoderm underwent radial intercalation and excessive thinning, which suggests that a cryptic radial cell intercalation behavior resists excessive convergence-driven mesodermal thickening in normal embryos. When unimpeded by convergence forces in *Ptk7* mutants, this unopposed radial intercalation resulted in excessive thinning of the mesoderm. These results show for the first time the polarized cell behaviors underlying CE in the mouse, demonstrate unique aspects of these behaviors compared with those of other vertebrates, and clearly define specific roles for planar polarity and for the novel planar cell polarity gene, *Ptk7*, as essential regulators of mediolateral cell intercalation during mammalian CE.

KEY WORDS: Gastrulation, Axial elongation, Morphogenesis, PTK7, Planar cell polarity, Mouse

INTRODUCTION

The morphogenetic movement of convergent extension (CE) plays key roles in early vertebrate morphogenesis. It extends the presumptive anterior-posterior (A/P) body axis during gastrulation and neurulation, and functions in other aspects of morphogenesis, such as blastopore closure in amphibians and primitive streak elongation in birds (Keller et al., 2000; Glickman et al., 2003; Voiculescu et al., 2007). Failure of CE results in gastrulation defects, notably failure of blastopore closure in amphibians (Schechtman, 1942; Keller, 1981; Keller, 1984), failure of A/P body axis elongation in frogs (Keller, 2002; Keller and Shook, 2008), fish (Myers et al., 2002; Glickman et al., 2003) and mice (Lu et al., 2004; Wang et al., 2006; Ybot-Gonzalez et al., 2007), and failure of neural tube closure in amphibians (Jacobson and Gordon, 1976; Wallingford and Harland, 2001; Goto and Keller, 2002) and mice (Lu et al., 2004; Wang et al., 2006; Ybot-Gonzalez et al., 2007). This central element of early morphogenesis is thus of great biomedical importance, particularly in understanding neural tube defects.

In amphibians, CE of the mesodermal and posterior neural tissues during gastrulation and neurulation drives early body axis elongation (Keller and Danilchik, 1988). Mediolateral intercalation of cells (MIB), driven by mediolateral bi-polarization of mesodermal cell motility (Keller and Tibbetts, 1989; Shih and Keller, 1992a; Shih and Keller, 1992b) and by medially directed cell motility in posterior neural tissues (Keller et al., 1992a; Elul and Keller, 2000; Ezin et al., 2003), produces a narrower, longer array of cells. In the fish, similar MIB (Kimmel et al., 1994; Myers et al., 2002) is driven by polarized motility in the notochord (Glickman et al., 2003) and dorsally directed migration in the lateral mesoderm (Trinkaus, 1998; Jessen et al., 2002; Lin et al., 2005). MIB appears to underlie CE during gastrulation and neurulation in birds (Schoenwolf and Alvarez, 1989; Alvarez and Schoenwolf, 1991; Schoenwolf and Alvarez, 1992) and mice (Smith et al., 1994; Sulik et al., 1994; Wang et al., 2006; Ybot-Gonzalez et al., 2007), where labeling cells shows cell intercalation of the notochord and neural plate (Sulik et al., 1994; Wang et al., 2006; Ybot-Gonzalez et al., 2007), although the underlying cell motility is unknown.

Non-canonical Wnt/planar cell polarity (PCP) signaling appears essential for polarization of the cell behaviors underlying CE in both the frog (Tada and Smith, 2000; Wallingford et al., 2000; Wallingford and Harland, 2001; Goto and Keller, 2002) and the zebrafish (Heisenberg et al., 2000; Sepich et al., 2000; Jessen et al., 2002). The Wnt/PCP pathway is similar to the *Drosophila* PCP pathway, which is essential for polarizing cells in the plane of the epithelium of the wing and the eye (Adler, 2002; Mlodzik, 2002). The core components of the *Drosophila* pathway include the atypical cadherin-like molecule, Flamingo (also known as Starry night), transmembrane proteins Frizzled and Van Gogh (also known as Strabismus), and cytoplasmic signaling proteins Dishevelled, Diego and Prickle. In *Xenopus* and zebrafish, perturbation of Dishevelled (Dsh) (Wallingford et al., 2000; Tada et al., 2002), Van Gogh (Darken et al., 2002; Goto and Keller, 2002), Prickle (Veeman et al., 2003), and Wnt5a and Wnt11 (Moon et al., 1993; Heisenberg et al., 2000; Smith et al., 2000) result in failure of CE and the underlying MIB, and in the case of Dsh and Van Gogh, failure of the underlying polarized protrusive activity (Wallingford and Harland, 2001; Voiculescu et al., 2007).

[1]Department of Cell Biology, University of Virginia Health System, Charlottesville, VA 22908, USA. [2]Department of Biology and [3]Keck Center for Cellular Imaging, University of Virginia, Charlottesville, VA 22903, USA. [4]Public Health Sciences, Division of Biostatistics and Epidemiology, University of Virginia Health System, Charlottesville, VA 22908, USA. [5]Department of Cell and Molecular Biology, Tulane University, New Orleans, LA 70118, USA.

*Author for correspondence (e-mail: as9n@virginia.edu)

Accepted 21 April 2009

Mutations of non-canonical Wnt/PCP pathway genes in the mouse, including *Van Gogh* (*Vangl1/Vangl2* – Mouse Genome Informatics) (Kibar et al., 2001; Murdoch et al., 2001; Montcouquiol et al., 2003; Torban et al., 2008), *flamingo* (*Celsr*) (Curtin et al., 2003), and *dishevelled* (*Dvl1/Dvl2*) (Wang et al., 2006) lead to short body axes, wide somitic mesoderm and neural plate, and an open neural tube. Mutations in the human gene for *Vangl1* are also associated with neural tube defects (Kibar et al., 2007). Mutations in the vertebrate genes *Ptk7* and *Scrb1* (*Scrib* – Mouse Genome Informatics), which are not core PCP genes in *Drosophila*, lead to similar defects and interact genetically with Wnt/PCP genes (Montcouquiol et al., 2003; Lu et al., 2004). These observations suggest that axial extension in the mouse may also occur by MIB, regulated by mechanisms similar to those in frog and fish.

Despite these conserved features, the mechanisms underlying CE in the mammal cannot be extrapolated from frogs, fish or flies, for several reasons. First, several different tissue- and stage-specific types of mediolaterally polarized cell behavior occur during vertebrate CE, and these differ between frogs and fish (Keller et al., 2000; Glickman et al., 2003; Lin et al., 2005). Second, in frogs and fish the active, force-producing cell intercalations occur by polarized protrusive activity among mesenchymal cells, whereas the cell intercalation observed in *Drosophila* occurs among epithelial cells, not by polarized protrusive activity but by polarized apical junctional remodeling (Keller, 2002; Blankenship et al., 2006). In the mouse, unlike frogs and fish, both epithelial (notochordal, neural) and mesenchymal (somitic) tissues undergo CE. Finally, the planar polarity of cell intercalation during CE of the *Drosophila* germband does not require the PCP pathway but instead requires A/P stripes of gene expression (Zallen and Wieschaus, 2004), whereas CE of the *Drosophila* hindgut requires unpaired (Upd, also known as outstretched) and STAT (Johansen et al., 2002; Lengyel and Iwaki, 2002). In contrast to its role in vertebrate CE, the *Drosophila* PCP pathway regulates the polarity of terminally differentiated structures, including the hairs in the wing, bristles on the body and ommatidial cell differentiation (Adler, 2002; Mlodzik, 2002)

Here we show via high-resolution imaging of living embryos that mouse mesodermal CE occurs by MIB, and that the first event in this process is mediolateral elongation and alignment of cells, followed by mediolaterally polarized cell motility and intercalation. Lack of PTK7 leads to failure of the initial polarization and to subsequent failure of CE. These results describe for the first time the cellular mechanisms underlying mammalian CE, and show that some aspects are unique and some are shared with other model systems. This characterization will guide future studies of cell polarity during CE and body axis formation.

MATERIALS AND METHODS

Animals

Animal-use protocols were reviewed and approved by the University of Virginia Institutional Animal Care and Use Committee, and were in compliance with PHS and USDA guidelines for laboratory animal welfare. Mice of strain Tg(GFPX)4Nagy/J containing an X chromosome-integrated *EGFP* transgene (Hadjantonakis et al., 2001) were obtained from The Jackson Laboratory (Bar Harbor, ME) and from Dr Terry Magnuson (University of North Carolina, Chapel Hill, NC, USA), and maintained as a heterozygous stock. For labeled *Ptk7* mutant mice, Tg(GFPX)4Nagy/J males were crossed with female XST87 mice, which carry a disrupted allele of the *Ptk7* gene (Lu et al., 2004). Females carrying both mutant *Ptk7* and *EGFP-X* alleles were backcrossed to XST87 males and the offspring were intercrossed to generate $Ptk7^{mu/mu}$ $EGFP\text{-}X^{+/-}$ embryos.

Embryos were dissected at 7.5 and 8.5 days post-coitum and those expressing EGFP were staged and oriented posterior side down on glass bottom culture dishes (see Fig. S1 in the supplementary material), secured with Nitex mesh and cultured in whole embryo culture medium [50% rat serum (Harlan Bioproducts for Science, Indianapolis, IN, USA) and 50% Eagle Plus medium (Stephens et al., 1995; Martin and Sutherland, 2001)] in a PDMI-2 stage heater (Harvard Apparatus, Holliston, MA, USA) at 37°C, with 5% CO_2. Sibling embryos in static culture in an incubator served as controls for normal development.

Immunofluorescence

For whole-mount immunostaining, embryos were fixed for 15 minutes in 3.7% formaldehyde, washed in PBS, permeabilized in 0.1% Triton X-100, blocked in 10% FBS/5% BSA overnight at 4°C, then incubated with rhodamine-phalloidin (Sigma, St Louis, MO, USA) and antibodies against brachyury (Santa Cruz Biotechnology, Santa Cruz, CA, USA) and either fibronectin (Millipore, Billerica, MA, USA) or PTK7 (Lu et al., 2004) for 1 hour at room temperature (RT). They were then washed in PBS, incubated with Alexa 350 anti-goat and Alexa 488 anti-rabbit antibodies (1 hour, RT), washed in PBS, mounted and analyzed by multiphoton microscopy at 740 nm excitation. All secondary antibodies were obtained from Invitrogen (Carlsbad, CA, USA). For sectional analysis, embryos were fixed as described above, then washed in PBS, infiltrated with a solution of cold water fish gelatin [15% cold water fish gelatin, 15% sucrose in PBS (Fagotto and Gumbiner, 1994)], embedded, frozen in liquid nitrogen and serially sectioned in the sagittal plane at 7 μm thickness.

Microscopy

EGFP-positive and immunostained embryos were examined using a BioRad Radiance 2100 laser scanning confocal/multiphoton microscope, consisting of: a Nikon TE300 epifluorescence microscope; a 100W mercury arc lamp; a BioRad Radiance 2100 confocal/multiphoton scanning system (Carl Zeiss Microimaging, Thornwood, NY, USA); an Argon Ion laser, a HeNe 543 laser; and a 10W Verdi pumped tunable, from 700-1000 nm (model 900 Mira, www.coherentinc.com), mode-locked ultrafast (78 MHz), pulsed (<150 femtosecond) laser. The system was equipped with a laser spectrum analyzer (Model E201; Mirion Technologies, San Ramon, CA, USA) to monitor the excitation wavelength, and a power meter to measure the laser power at the specimen plane (Model SSIM-VIS & IR; Coherent, Santa Clara, CA, USA) (Chen and Periasamy, 2004). Excitation wavelengths of 488 nm for EGFP and 740 nm for multiphoton imaging were used. Plan Fluor 20× NA 0.75 multi-immersion, Plan Apo 40× NA 1.0 oil and C Apo 40× NA 1.15 water immersion objectives were used for laser scanning confocal image acquisition. LaserSharp2000 software was used to acquire both confocal and multiphoton images using the three internal detectors and also for the transmission detector. Scanning confocal image stacks were taken at 4-minute intervals for 20× time-lapse movies, and at 2-minute intervals for 40× time-lapse movies. Each stack consisted of approximately 17 or 12 sections, respectively, each 4 μm apart. Multiphoton image stacks consisted of approximately 110 sections, 1 or 0.2 μm apart.

Image analysis

Confocal and multiphoton data were analyzed using Volocity and Openlab (Improvision, Waltham, MA, USA) and ImageJ (NIH, Bethesda, MD, USA) software. The images were divided into three regions relative to the posterior notochord (PNC) (Blum et al., 2007) and notochordal plate, with the midline defined by a line through the middle of the PNC and along the notochordal plate. Region 1 is posterior to the PNC and contains cells in the primitive streak (anterior primitive streak), region 2 is lateral to the PNC and contains posterior presomitic mesoderm, and region 3 is lateral to the notochord and posterior to the last-formed somite, and contains anterior presomitic mesoderm. Cells from each region in seven different embryos were traced, and the length of the longest axis and its longest perpendicular axis, and the angle of the longest axis relative to the midline of the image were determined. The angle measurement was corrected for any deviation of the embryonic A/P axis from the image midline. These data were used to calculate the aspect (length to width) ratio and angle of orientation relative to the A/P axis for each cell examined. Repeated measures models were used to compare aspect ratios and distortion measurements of cells across *Ptk7*

mutant and wild-type (WT) embryos. These models allow for correlations between cells measured from the same embryo. F-tests in these models were used to make specific comparisons on how measurements differed by section in WT and *Ptk7* mutant embryos.

Protrusive activity was analyzed for 10-29 cells in each defined sector of the embryo using OpenLab (Improvision). Each protrusion observed over a 4-hour period was marked using the cell-counter tool. The angular distribution of the observed protrusions was determined by counting the number of protrusions that fell into each of 12 sectors (of 30°) of a circle around the cell perimeter, the center of which corresponded to the center of the cell. The 90°/270° axis was aligned with the A/P axis of the embryo. The average distribution of protrusions was determined by combining observations for all cells in each defined sector surrounding the PNC, and were analyzed as described previously (Elul and Keller, 2000; Ezin et al., 2003; Ezin et al., 2006), using a χ^2 test to determine whether the distribution of protrusive activity was significantly different from random and the 2ai test (Baschelet, 1981; Zar, 1998) to determine whether they were monopolar or bipolar (Ezin et al., 2003). We computed 'preferred directions' of protrusion in a given section of the embryo by comparing the frequency of observed protrusion directions by a cell to that expected by chance, and permutation tests were used to assign a probability to the observed difference. If the probability in one direction was less than 0.05, the cell was designated as preferring one direction or 'monopolar'. If the probability in two directions was less than 0.05, and the preferred directions were approximately 180° apart, the cell was designated as 'bipolar'. In all other cases, the cell was designated as having no preferred direction, or 'multipolar'. χ^2 tests were used to compare frequency of cells labeled as 'monopolar', 'bipolar' and 'multipolar' across sections.

Radial movement of cells was assessed by counting, during a 2-hour time-lapse sequence, the number of cells that disappeared from or appeared into a 12-16 μm thick region (3-4 summed confocal *z*-sections) located 12 μm deep to the surface endoderm layer. Between 30 and 34 measurements were taken on regions 2 and 3 of eight WT embryos, and 24 measurements were taken on regions 2 and 3 of six *Ptk7* mutant embryos. The measurements were averaged, and analyzed for statistical significance by ANOVA followed by the Student-Newman-Keuls test.

The thickness of the presomitic mesoderm was examined in WT and *Ptk7* mutant embryos by the direct measurement of sagittal sections of embryos. The first three sections on either side of the notochord (total of six sections) were selected for each of three embryos of each genotype (WT and *Ptk7* mutant), and the region posterior to the last segmented somite was measured in each section. The measurements were averaged and evaluated for statistical significance by ANOVA.

RESULTS

Paraxial and axial mesoderm are shorter and wider in *Ptk7* mutant embryos than in wild-type embryos

Morphology of WT and *Ptk7* mutant embryos at late streak, headfold, and 5-7 somites was compared by laser scanning confocal microscopy of fluorescent marker staining. In WT embryos, the primitive streak forms in the proximal posterior region of the epiblast, and elongates until it reaches the distal tip of the embryo at the late streak stage (Fig. 1A). Elevation of the neural folds and invagination of the foregut pocket follow (Fig. 1A), along with condensation of the somites as pairs of rectangular, nearly square blocks of tissue along both sides of the neural tube (Fig. 1B, S). The elongation of the primitive streak culminates in the formation, at the late streak/early headfold stage, of an oval, bilayered structure composed of columnar epithelial cells located at the anterior end of the primitive streak (Fig. 1B, PS). This structure has commonly been designated as the node, but more recent evidence has corrected its designation to the posterior notochord (PNC) (Blum et al., 2007), which is continuous anteriorly with the notochordal plate (Fig. 1B, not) and floor plate of the neural tube (Sulik et al., 1994). The region surrounding the PNC consists of presumptive somitic cells (Fig. 1B, PreS) (Kinder et al., 1999).

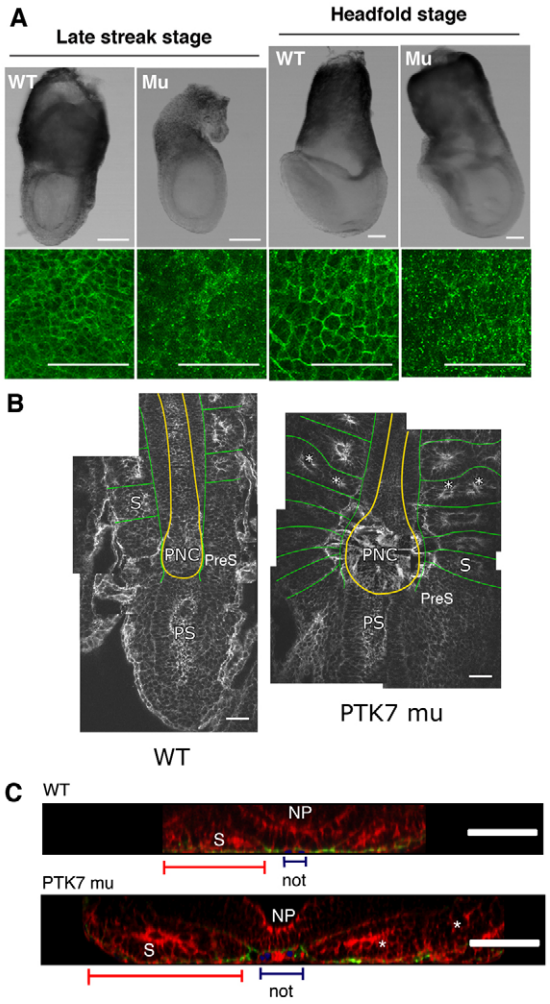

Fig. 1. Morphology of axial and paraxial structures. (**A**) Brightfield images (upper row) of WT and mutant mouse embryos at late streak and early headfold stages. Confocal images (lower row) show membrane localization of PTK7 in the WT embryos and diffusely localized dots of the truncated mutant protein in the *Ptk7* mutant embryos. Anterior is to the left. (**B**) Montage confocal images of WT and *Ptk7* mutant fixed embryos stained with rhodamine-phalloidin. The superficial boundaries between the notochordal plate and somitic tissues are shown with orange lines and the deeper boundaries between the neural plate and somitic tissue and between formed somites are shown with green lines. Asterisks indicate somitic cavities. Anterior is up. (**C**) Optical cross-sections at the level of the most posteriorly formed somite in fluorescently stained embryos. Blue, antibody against brachyury; green, antibody against fibronectin; red, f-actin detected by phalloidin staining. PS, primitive streak; NP, neural plate, PNC, posterior notochord; not, notochordal plate; PreS, presomitic mesoderm; S, somite. Scale bars: 100 μm.

Homozygous *Ptk7* mutant embryos were morphologically indistinguishable from WT prior to early somite stages, with normal formation of the primitive streak, head folds and foregut (Fig. 1A). By the 5-somite stage, however, *Ptk7* mutants were shorter and wider than WT or heterozygous littermates (Lu et al., 2004), and the PNC and notochordal plate were significantly wider than in WT embryos (Fig. 1B and Fig. 2; see Fig. S2 in the supplementary material). The somites of *Ptk7* mutant embryos were shorter in the A/P dimension, wider mediolaterally (Fig. 1B) and compressed into

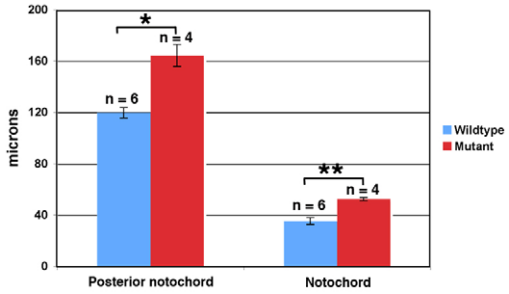

Fig. 2. Difference in width of posterior notochord and notochord. The width of the posterior notochord and notochord are significantly increased in *Ptk7* mutant embryos (one-way ANOVA, **P*<0.00001; ***P*<0.000001). Data show the mean±s.e.m.; *n*=6 embryos for WT, *n*=4 embryos for *Ptk7* mutants.

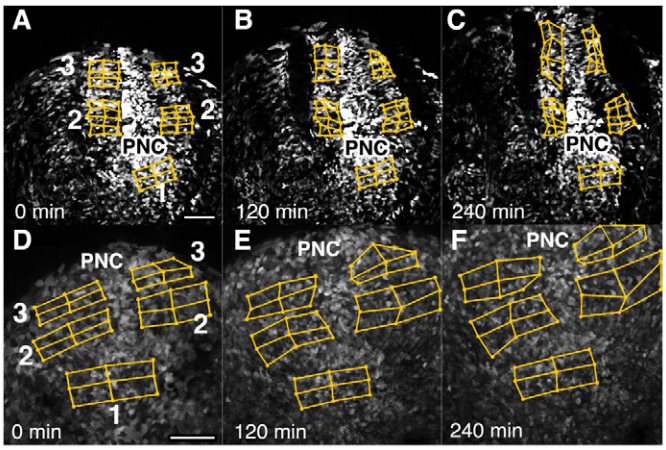

Fig. 3. Patterns of tissue distortion during CE in WT and *Ptk7* mutant embryos based on time-lapse confocal imaging. Distortion diagrams show that, over a 4-hour period, regions 2 and 3 in WT embryos (**A-C**) converge and extend in the A/P axis, whereas region 1 does not. By contrast, regions 2 and 3 of *Ptk7* mutant embryos (**D-F**) become wider mediolaterally and do not extend. The numbers in A and D indicate the region represented by each box. Anterior is up; PNC, posterior notochord. Scale bars: 100 μm.

a limited space along the presumptive A/P axis, with the last somite pair formed directly adjacent to the PNC (S) (Fig. 1B). This is substantially more posterior to the position of the last somite pair in WT littermates, making the presomitic mesoderm very short in the A/P axis, and very wide mediolaterally. Somites in *Ptk7* mutant embryos did epithelialize and cavitate, but they either formed several, separated cavities or one mediolaterally elongated cavity (asterisks, Fig. 1B,C; see Fig. S2 in the supplementary material).

The presomitic mesoderm undergoes CE in WT but not in *Ptk7* mutant embryos

To examine CE in paraxial mesoderm, we mapped tissue shape changes in three regions: region 1, consisting of the primitive streak region posterior to the PNC; region 2, the presomitic mesoderm lateral to the PNC; and region 3, the presomitic region anterior to the PNC and posterior to the somites. Tissue distortions were mapped by tracking the movements of individual mesodermal cells lying at the intersects of grid patterns over a 4-hour period in time-lapse movies of WT embryos (Fig. 3A-C) and *Ptk7* mutant embryos (Fig. 3D-F). In WT and heterozygous embryos, regions 2 and 3 progressively lengthened and narrowed over 4 hours, whereas region 1 remained relatively unchanged (Fig. 3A-C). By contrast, in *Ptk7* mutant embryos all three regions retained their initial shape and instead increased in area more-or-less uniformly in all directions (Fig. 3D-F). Thus CE of the presomitic mesoderm is impaired in embryos that lack *Ptk7*.

Presomitic cells of WT embryos become mediolaterally elongated and oriented as they move anteriorly past the PNC but those of *Ptk7* mutant embryos do not

Cell shapes differed between the three regions defined above. In region 1 the mean aspect ratio was 1.4, whereas mean aspect ratios were significantly higher in regions 2 and 3, at 2.4 and 2.6, respectively (Fig. 4A). WT presomitic cells also became oriented in region 2. In region 1 the long axes of the cells were randomly oriented relative to the midline (Fig. 4B), but cells in region 2 were oriented with their longest axis at a ~60° angle relative to the midline (Fig. 4B), whereas in region 3 the orientation of the longest axes of these cells was essentially perpendicular to the midline (Fig. 4B).

By contrast, mesoderm cells in *Ptk7* mutant embryos showed no shape change between regions 1, 2 and 3 (Fig. 4A). Aspect ratios for *Ptk7* mutant cells in all regions were similar to those of region 1 in WT embryos (Fig. 4A). *Ptk7* mutant cells also failed to become oriented; the long axes of the cells in regions 2 and 3 remained randomly oriented (Fig. 4B, *Ptk7* mutant). The failure of cell elongation and orientation in regions 2 and 3, regions that also fail to display CE in *Ptk7* mutant embryos, strongly suggests that the polarization of cells as they exit the primitive streak is an essential element in the development of CE behavior.

PTK7 affects polarized protrusive activity and intercalation behavior

To determine whether polarized protrusive activity and mediolateral intercalation behavior (MIB) underlies CE in mouse mesoderm, we examined protrusive activity and displacement of mesodermal cells in the regions described above. Individual cells were tracked through 5-hour time-lapse projections (12 μm depth) (Fig. 5), and protrusions made by these cells were marked, binned and summed in rose diagrams representing the angular distributions of their frequencies (Fig. 6). The overall rate of protrusive activity was not significantly different between WT (42.54 protrusions/hour/cell) and *Ptk7* mutant cells (43.62 protrusions/hour/cell). Cells in region 1 of WT embryos moved by directed migration with high persistence (infrequent change of direction), in an anterior and lateral direction (Fig. 5A; see Movie 1 in the supplementary material). These cells showed multipolar protrusive activity directed nonrandomly in lateral and anterior directions, but were also significantly more likely to exhibit monopolar protrusive activity (Fig. 6A). Thus the behavior of WT cells in region 1 is a canonical directed migration in which the dominant direction of protrusive activity coincides with the direction of cell translocation.

By contrast, cells in regions 2 and 3 moved very differently. At the outset in region 2, the cells showed decreased persistence and reversed their direction in the mediolateral axis relatively often, creating a zigzag pattern of local movement characterized by large lateral and medial excursions and a large number of neighbor changes (Fig. 5B; see Movie 2 in the supplementary material). Cells in region 2 also exhibited multipolar protrusive activity, but were significantly less likely to exhibit monopolar protrusive activity than

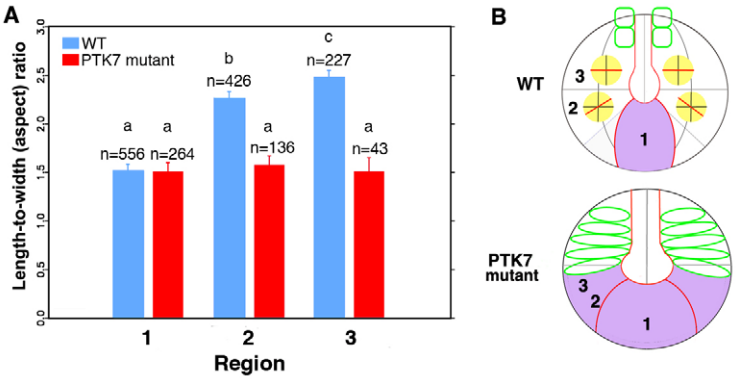

Fig. 4. Shape and orientation of presomitic cells in live WT and *Ptk7* mutant embryos. (**A**) Average aspect ratios of cells in regions 1, 2 and 3 of WT and *Ptk7* mutant embryos. Data show the mean±s.e.m. The numbers of cells analyzed are listed above each bar, and were from seven WT embryos and four *Ptk7* mutant embryos. Bars labeled with different letters are significantly different from one another, $P<0.0001$ in each case. (**B**) Schematic representing the mean orientation of the long axis of the cells in each of the different regions analyzed (red line) in reference to the A/P and mediolateral axes of the embryo (gray lines within the yellow circles). In the regions colored purple the long axes of the cells are randomly oriented. Anterior is up.

those in region 1 (Fig. 6A). Further anteriorly in region 3, cells showed local, conservative neighbor changes (cell intercalation), without the medial and lateral excursions characteristic of cells in region 2, with persistent anterior displacement and separation along the A/P axis (Fig. 5C; see Movie 3 in the supplementary material). These cells were strongly bipolar in their protrusive activity, and this activity was oriented mediolaterally (Fig. 6). Although they maintained a consistent, anterior-directed displacement, it was produced by mediolaterally biased protrusive activity, mediolateral intercalation and convergence leading to anterior extension, rather than by anteriorly directed migration. In region 3, the behavior of cells is a canonical MIB, where the dominant direction of protrusive activity is perpendicular to the direction of translocation.

In *Ptk7* mutant embryos, cells in region 1 showed the same type of anteriorly and laterally directed displacement of high persistence seen in WT embryos, through anteriorly and laterally biased multipolar protrusive activity (Figs 5 and 6). However, this behavior continued unaltered in the compressed regions 2 and 3 lateral to the PNC and posterior to the last segmented somite, and there were no changes in the angular distribution of protrusions between these regions (Fig. 6). All cells examined in the *Ptk7* mutant equivalent of region 3 exhibited monopolar or multipolar protrusive activity, similar to region 1 (Fig. 6). The cells in regions 2 and 3 continued to move using anteriorly and laterally directed migration, and never exhibited the regional behaviors seen in the WT of either the large medial and lateral excursions (region 2) or the final phase of highly mediolaterally polarized protrusive activity (region 3) (Fig. 5D; see Movie 4 in the supplementary material), nor do they undergo mediolateral cell intercalation (Fig. 5E). To determine whether there were any earlier differences in protrusive activity of mesodermal cells, we examined cells within the primitive streak of WT and *Ptk7* mutant embryos at E7.5. At this stage the displacement and the protrusive behavior of cells in *Ptk7* mutant embryos were indistinguishable from those of WT embryos (Fig. 6).

Radial intercalation (intercalation perpendicular to the tissue plane) is often paired with mediolateral intercalation (within the tissue plane) to regulate the three-dimensional shape change of the tissue (Keller et al., 2008; Yin et al., 2008). We examined the rate of radial intercalation by determining the number of cells per unit time that disappeared (negative radial intercalation) or appeared (positive radial intercalation) into a 12-16 μm region located 12 μm deep to the surface endoderm. In WT embryos, cells disappeared predominantly in the middle and at the lateral edges of both regions 2 and 3 at an average rate of about six cells per 2-hour period, and appeared at an average rate of less than one cell per 2-hour period, suggesting that the tissue is thickening by generating new, intermediate layers of fewer cells per layer (Fig. 7). In surprising contrast, whereas *Ptk7* mutant embryos showed similar numbers of cells disappearing from the observed layer in regions 2 and 3, they had a rate of appearance of almost six cells per 2-hour period (Fig. 7). Thus, whereas WT presomitic mesoderm has a net negative radial intercalation, *Ptk7* mutant presomitic mesoderm has no net change in the number of cells within the plane of the observed region, which should lead to a thinner tissue of greater area in the mutant embryo.

To examine this issue, we measured the thickness of the presomitic mesoderm at three separate points within the first 25 μm on either side of the notochord (total of six measurements per embryo, three embryos each of WT and *Ptk7* mutant). The average thickness of the presomitic mesoderm in the *Ptk7* mutant embryo (75.3 μm) was indeed significantly less than that of the WT (112.8 μm) (Fig. 8).

PTK7 has no effect on Dvl2 localization

Activation of the non-canonical Wnt/PCP pathway is thought to involve localization of DVL to the plasma membrane (Wallingford et al., 2000), and this is supported by findings that DVL localization is altered in PCP mutants (Yin et al., 2008) and after impairment of PTK7 function (Shnitsar and Borchers, 2008). However, staining of embryos with antibodies against DVL2, which, of the three DVL proteins in the mouse, plays a dominant role in neural tube closure (Wang et al., 2006; Etheridge et al., 2008), revealed no differences in the localization of DVL2 to the plasma membrane between WT and *Ptk7* mutant embryos in the axial or paraxial mesoderm, or in the primitive streak (see Fig. S3 in the supplementary material). Nor were any differences seen in the localization of actin, myosin IIa, or myosin IIb in the presomitic mesoderm of the *Ptk7* mutant or WT embryos (see Fig. S3 in the supplementary material). Thus PTK7 does not appear to affect gross aspects of DVL2 distribution or of cytoskeletal organization.

DISCUSSION

The results presented here characterize for the first time the normal pattern of mesodermal cell behavior during CE of the mouse body axis. Prospective somitic mesoderm cells initially exhibit multipolar, biased protrusive activity resulting in migration laterally and anteriorly from the anterior primitive streak, but then elongate and aligns with the presumptive mediolateral axis of the tissue and polarized their protrusive activity mediolaterally, leading to a high degree of local mediolateral intercalation and CE. Throughout this progression the cells are displaced anteriorly; initially anterior displacement are driven directly by anteriorly directed protrusive activity, and subsequently are driven indirectly by mediolaterally polarized protrusive activity and MIB.

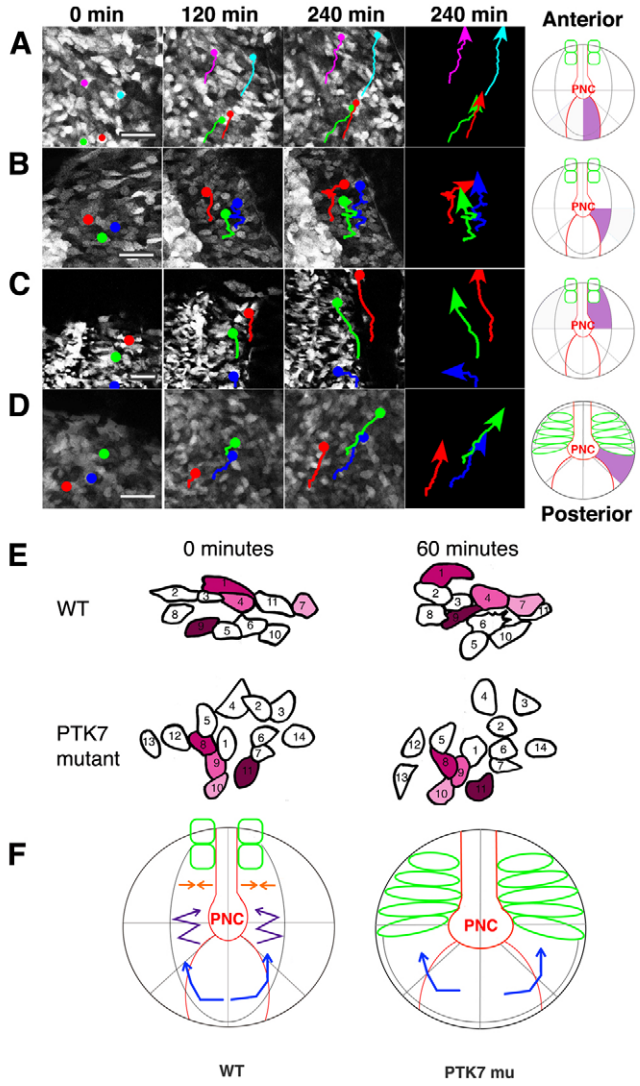

Fig. 5. Patterns of cell movement in paraxial mesoderm. Tracks of individual cell movements over a 4 hour period in the WT region 1 (**A**), WT region 2 (**B**), WT region 3 (**C**) and tracks that represent cells in both regions 2 and 3 of *Ptk7* mutant embryos (**D**). Diagrams at the end of each row indicate the specific regions of the embryo from which these images were taken (purple). Scale bar: 50 μm. Anterior is up; PNC, posterior notochord. (**E**) Diagram of the positions of individual labeled cells in WT and *Ptk7* mutant embryos at the start and end of a 1 hour interval in a time-lapse sequence. (**F**) Schematic representing movements of cells in the primitive streak (blue), transitional (purple) and presomitic (orange) regions of WT and *Ptk7* mutant embryos. Anterior is up.

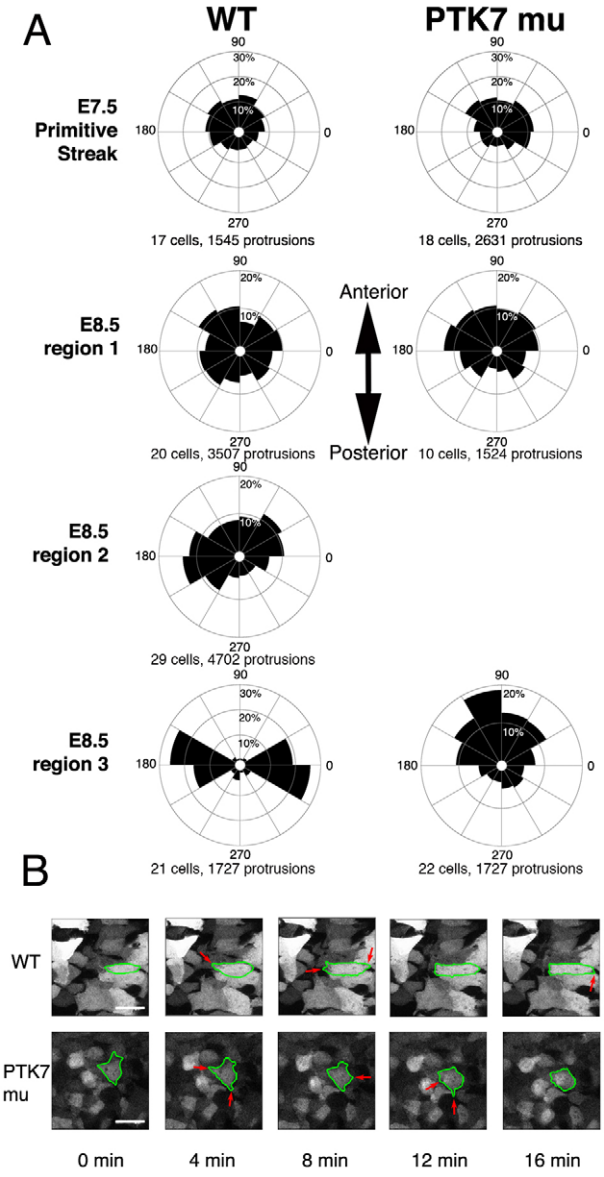

Fig. 6. Distribution of protrusive activity. (**A**) Rose diagrams show the distribution of protrusive activity of cells in the E7.5 primitive streak, and in regions 1, 2 and 3 of E8.5 WT embryos compared with cells in the corresponding regions of *Ptk7* mutant embryos. Cell behavior was identical in regions 2 and 3 of the *Ptk7* mutant, and is represented by the single rose diagram for region 3. Data are represented as the mean percentage of total protrusions that occur in each bin, and the total number of cells and protrusions analyzed are listed under each diagram. Data are from six WT embryos and four *Ptk7* mutant embryos. The 90°/270° line represents the A/P axis of the embryo. (**B**) Frames from time-lapse sequences, showing motile cells in region 3 of WT (top) and *Ptk7* mutant (bottom) embryos. Individual cells are outlined in green, red arrows point to protrusions. Scale bars: 20 μm.

MIB in the mouse increases progressively along the A/P axis, and the major transition in polarized cell behavior occurs lateral to the PNC as the cells leave the streak, paralleling the post-involution transition to MIB in the frog. It results in CE of the tissue, and occurs in the same relative location and orientation with respect to the notochord and last-segmented somites (Wilson et al., 1989; Shih and Keller, 1992b). However, MIB in the mouse mesoderm follows an epithelial to mesenchymal transition (EMT) in the streak, and anterior- and lateral-directed cell migration, behaviors not seen prior to MIB in the frog. In the zebrafish, presumptive somitic mesoderm undergoes a post-involution, dorsally directed, Gα12/13-dependent migration that is followed by a Wnt/PCP-dependent MIB and CE (Sepich et al., 2000; Lin et al., 2005; Sepich et al., 2005; Yin et al., 2008).

Unique to mouse MIB are the significant elongation and alignment of cells prior to the onset of strongly biased protrusive activity. In the frog, the mediolateral bias of protrusive activity

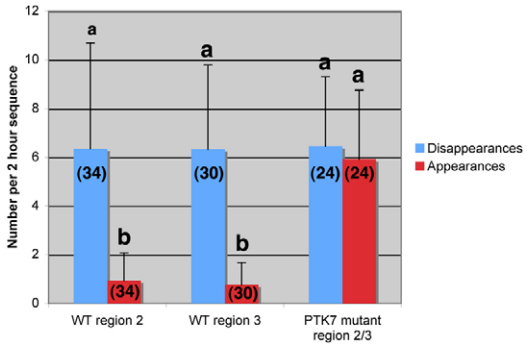

Fig. 7. Radial cell movement in paraxial mesoderm. Graph showing the numbers of cells that moved in or out of a 12-16 µm region, located 12 µm deep to the surface endoderm, during a 2-hour time-lapse sequence. Data are represented as the mean±s.d.; numbers on each bar represent the number of observations made on *n*=8 embryos for WT and *n*=6 embryos for the *Ptk7* mutant. Bars marked with different letters are significantly different from one another (one-way ANOVA followed by the Student-Newman-Keuls test, *P*>0.01).

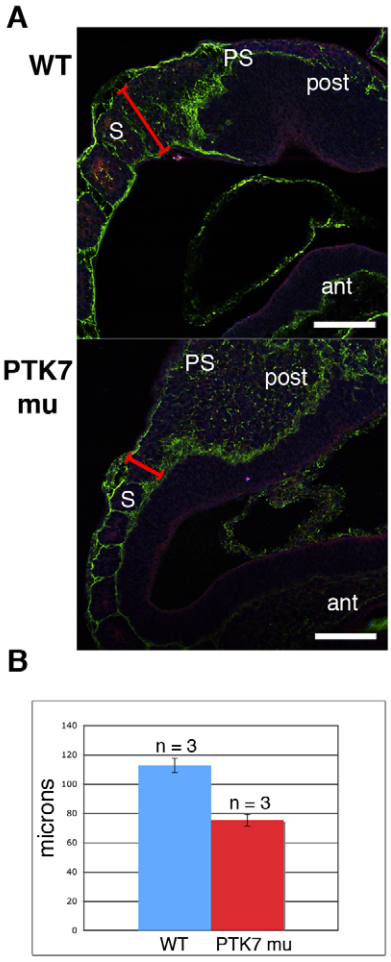

Fig. 8. Comparison of the thickness of presomitic mesoderm. (**A**) Confocal images of representative sagittal sections from which measurements were taken. Sections were immunostained with phalloidin (red) and an antibody against fibronectin (green). The red bar indicates the region where measurements were taken. Six sections from each of three separate embryos for each genotype (WT and *Ptk7* mutant) were analyzed. Ant, anterior; post, posterior; PS, primitive streak; S, most posterior formed somite. Scale bars: 100 µm. (**B**) The average thickness of the presomitic mesoderm of the *Ptk7* mutant is significantly less than that of the WT (*P*<0.00001 by one-way ANOVA).

occurs simultaneously with mediolateral cell elongation and alignment (Shih and Keller, 1992a; Shih and Keller, 1992b), and the causal relationship between the two has never been determined. Extreme cell elongation occurs in explants in which intercalation is mechanically frustrated, arguing that polarized traction on other cells or extracellular matrix puts the cells under mediolateral tension, thus driving elongation (Keller et al., 1992b; Keller and Shook, 2008), but the initial elongation may still be due to internally driven cell shape change rather than polarized traction.

Additionally, mouse somitic mesoderm shows a phase of 'zigzag' movement, in which cell movement is characterized by unusually large medial and lateral excursions with an overall anterior trajectory, a behavior not seen in *Xenopus* mesoderm. However, *Xenopus* deep neural plate cells express an abnormal, bipolar mode of intercalation under experimental conditions in which their bipolarity is statistically balanced over time, but tends to be unbalanced in the short term, resulting in excursions first one way and then the other (Elul et al., 1997; Elul and Keller, 2000; Keller et al., 2008). We interpret the zigzag behavior in the mouse as being a similar temporary imbalance, as the cells reorient their protrusive activity from the predominantly multipolar/monopolar distribution of the primitive streak to the definitive bipolar distribution driving MIB.

The roles that these cell behaviors play in driving axial extension are clarified in the *Ptk7* mutant embryo. In the absence of PTK7, the anteriorly directed migration of the somitic mesoderm is unaffected, whereas the strong MIB and CE seen in region 3 of the WT do not occur in the *Ptk7* mutant. This suggests that the initial migration behavior, unlike the dorsally directed migration in fish mesoderm, does not contribute to CE, and that MIB is the primary cellular mechanism of mouse mesodermal cell intercalation and CE. Whether the anterior-directed migration of mouse paraxial mesoderm is mechanistically similar to the Gα12/13-mediated dorsal migration of zebrafish cells (Lin et al., 2005), or to the FGF-dependent migration of chick mesodermal cells (Yang et al., 2002), remains to be seen.

The failure of polarized cellular behaviors and MIB in the absence of PTK7 leads to a shorter, wider body axis, similar to *Vangl2* or *Dvl1 Dvl2* mutant mouse embryos, in which defects in neural tube and notochord elongation and CE have been described (Wang et al., 2006; Ybot-Gonzalez et al., 2007). *Vangl2* and *Ptk7* do interact genetically, as compound heterozygotes exhibit a more severe phenotype than either single heterozygote (Lu et al., 2004). However, the phenotype of the compound heterozygote is also unlike that of either single homozygote, suggesting that the two genes may act in separate pathways that both affect axial extension and neural tube closure. In this context it is interesting that the *Ptk7* mutation appears to have a stronger effect on paraxial mesoderm cell behavior than either the *Vangl2* mutation or the *Dvl1 Dvl2* double knockout. Embryos homozygous for the *Ptk7* mutation have obvious defects in axial elongation and somite morphology by the 5-7 somite stage, whereas *Vangl2* mutant embryos exhibit normal axial elongation during this period (Gerrelli and Copp, 1997), and *Dvl1 Dvl2* double mutants have a shortened axis but have comparatively normal somite morphology (Wang et al., 2006). This may be due to compensating functions of VANGL1 and DVL3

proteins in the paraxial mesoderm, or it may be that PTK7 has a unique activity in the paraxial mesoderm. Such is the case in the zebrafish for the Gα12/13 proteins, which function earlier than the core Wnt/PCP proteins in a pathway parallel to the Wnt/PCP pathway, but affect cell behavior and tissue morphogenesis similarly to the core Wnt/PCP proteins (Lin et al., 2005).

The lack of PTK7 has a dramatic effect on axial morphogenesis, but a discrete effect on individual cell behavior: PTK7 specifically affects the polarization of the presomitic mesoderm relative to the midline of the embryo, and the subsequent onset of MIB. The directed migration and protrusive behavior of cells within the primitive streak is unaffected, and the prospective somitic mesoderm cells exhibit normal directed migration as they leave the streak. The lack of PTK7 does not affect cell fate or somitogenesis; somites condense and epithelialize similarly to WT, albeit with a different (wider) morphology owing to the lack of CE. These findings argue that PTK7 is a specific regulator of cell polarity rather than a general regulator of cell motility or cell fate.

The molecular mechanisms underlying this polarization process are not yet understood. PTK7 is a pseudokinase and thus is unlikely to be signaling directly by phosphorylation (Boudeau et al., 2006). A recent study implicated the kinase domain of PTK7 in the formation of a membrane-bound complex with Dsh and Frizzled 7 in the frog (Shnitsar and Borchers, 2008), whereby activation of the PCP pathway involves membrane localization of Dsh (Wallingford and Harland, 2002). However, DVL does not have a polarized distribution in mouse neuroepithelium, nor is its membrane localization affected by mutations in *Vangl2* (Wang et al., 2006). We also find that DVL2 distribution is not polarized in mouse mesodermal cells, and its membrane localization is not affected by PTK7. The absence of gross changes in the actomyosin cytoskeleton of PTK7 mutants reported here also suggests that PTK7 has a very specific function in polarity. Clearly much additional work is necessary to understand the molecular mechanisms regulating Wnt/PCP signaling during axial elongation, the potential mechanistic differences between species and the molecular mechanisms underlying cell polarization by PTK7.

The abnormal thinning of the paraxial mesoderm in the *Ptk7* mutant suggests that forces generated by radial intercalation normally oppose the tendency for convergence forces to thicken, as well as elongate, the tissue. In the frog, several lines of evidence suggest that tissue convergence, driven by mediolateral intercalation, produces compressive forces both along the A/P axis to produce extension, and in the radial axis to produce thickening (Keller and Tibbetts, 1989; Wilson and Keller, 1991; Keller et al., 2008). Such thickening is opposed by a tissue-thinning force generated by radial intercalation, and its magnitude regulates the relative amounts of extension and thickening that result from convergence (Keller and Tibbetts, 1989; Wilson and Keller, 1991; Keller et al., 2008). Alternatively, A/P polarization of radial intercalation can lead synergistically to increased extension, as shown in a recent study of the paraxial mesoderm of the zebrafish (Yin et al., 2008). Our results show that in the mouse the balance of radial movement in the presomitic mesoderm is negative, thus the tissue normally undergoes substantial radial thickening at the same time as it is converging and extending. In the absence of PTK7 there is no net radial movement of presomitic mesoderm cells, leading to abnormal thinning and lateral expansion of the tissue. As a result, the presomitic mesoderm and somites are thinner in the dorsal-ventral axis, broader in the mediolateral axis, and shorter in the A/P axis. Unfortunately, owing to the nature of the EGFP expression in the embryos used in this study we could not observe the relative position of all of the cells surrounding those that were moving in the radial direction, and thus were unable to determine whether the radial intercalation was polarized in either the A/P or mediolateral axis, and this remains as an important question to be addressed.

In summary, mesodermal CE in the mouse embryo is driven by polarized cell protrusive activity, the polarity of which is established through a PTK7-dependent event that occurs as the cells leave the primitive streak. Without this polarization the mesoderm cells fail to polarize their protrusive activity and develop MIB, and continue instead to undergo directed migration laterally and anteriorly. Concomitant, unopposed radial intercalation further broadens the somitic mesoderm field, and the resulting somites are mis-shapen in all axes as well as malpositioned along the A/P axis, leading to a shortened body axis posterior to the midbrain.

The authors acknowledge other members of their laboratories for helpful discussions of the data. This study was supported by NIH grants HD034807 to A.S. and DC009238 to X.L. W.W.Y. and M.W. received support from NIH Training Grants T32-HD07528 and T32-GM08136-23, respectively. Deposited in PMC for release after 12 months.

Supplementary material

Supplementary material for this article is available at http://dev.biologists.org/cgi/content/full/136/12/2039/DC1

References

Adler, P. N. (2002). Planar signaling and morphogenesis in Drosophila. *Dev. Cell* **2**, 525-535.

Alvarez, I. S. and Schoenwolf, G. C. (1991). Patterns of neurepithelial cell rearrangement during avian neurulation are determined prior to notochordal inductive interactions. *Dev. Biol.* **143**, 78-92.

Baschelet, E. (1981). *Circular Statistics in Biology*. London: Academic Press.

Blankenship, J. T., Backovic, S. T., Sanny, J. S., Weitz, O. and Zallen, J. A. (2006). Multicellular rosette formation links planar cell polarity to tissue morphogenesis. *Dev. Cell* **11**, 459-470.

Blum, M., Andre, P., Muders, K., Schweickert, A., Fischer, A., Bitzer, E., Bogusch, S., Beyer, T., van Straaten, H. W. and Viebahn, C. (2007). Ciliation and gene expression distinguish between node and posterior notochord in the mammalian embryo. *Differentiation* **75**, 133-146.

Boudeau, J., Miranda-Saavedra, D., Barton, G. J. and Alessi, D. R. (2006). Emerging roles of pseudokinases. *Trends Cell Biol.* **16**, 443-452.

Chen, Y. and Periasamy, A. (2004). Characterization of two-photon excitation fluorescence lifetime imaging microscopy for protein localization. *Micr. Res. Tech*. **63**, 72-80.

Curtin, J. A., Quint, E., Tsipouri, V., Arkell, R. M., Cattanach, B., Copp, A. J., Henderson, D. J., Spurr, N., Stanier, P., Fisher, E. M. et al. (2003). Mutation of Celsr1 disrupts planar polarity of inner ear hair cells and causes severe neural tube defects in the mouse. *Curr. Biol.* **13**, 1129-1133.

Darken, R. S., Scola, A. M., Rakeman, A. S., Das, G., Mlodzik, M. and Wilson, P. A. (2002). The planar polarity gene strabismus regulates convergent extension movements in Xenopus. *EMBO J.* **21**, 976-985.

Elul, T. and Keller, R. (2000). Monopolar protrusive activity: a new morphogenic cell behavior in the neural plate dependent on vertical interactions with the mesoderm in Xenopus. *Dev. Biol.* **224**, 3-19.

Elul, T., Koehl, M. A. and Keller, R. (1997). Cellular mechanism underlying neural convergent extension in Xenopus laevis embryos. *Dev. Biol.* **191**, 243-258.

Etheridge, S. L., Ray, S., Li, S., Hamblet, N. S., Lijam, N., Tsang, M., Greer, J., Kardos, N., Wang, J., Sussman, D. J. et al. (2008). Murine dishevelled 3 functions in redundant pathways with dishevelled 1 and 2 in normal cardiac outflow tract, cochlea, and neural tube development. *PLoS Genet*. **4**, e1000259.

Ezin, A. M., Skoglund, P. and Keller, R. (2003). The midline (notochord and notoplate) patterns the cell motility underlying convergence and extension of the Xenopus neural plate. *Dev. Biol.* **256**, 100-114.

Ezin, A. M., Skoglund, P. and Keller, R. (2006). The presumptive floor plate (notoplate) induces behaviors associated with convergent extension in medial but not lateral neural plate cells of Xenopus. *Dev. Biol.* **300**, 670-686.

Fagotto, F. and Gumbiner, B. M. (1994). Beta-catenin localization during Xenopus embryogenesis: accumulation at tissue and somite boundaries. *Development* **120**, 3667-3679.

Gerrelli, D. and Copp, A. J. (1997). Failure of neural tube closure in the loop-tail (Lp) mutant mouse: analysis of the embryonic mechanism. *Brain Res. Dev. Brain Res.* **102**, 217-224.

Glickman, N. S., Kimmel, C. B., Jones, M. A. and Adams, R. J. (2003). Shaping the zebrafish notochord. *Development* **130**, 873-887.

Goto, T. and Keller, R. (2002). The planar cell polarity gene strabismus regulates convergence and extension and neural fold closure in Xenopus. *Dev. Biol.* **247**, 165-181.
Hadjantonakis, A. K., Cox, L. L., Tam, P. P. and Nagy, A. (2001). An X-linked GFP transgene reveals unexpected paternal X-chromosome activity in trophoblastic giant cells of the mouse placenta. *Genesis* **29**, 133-140.
Heisenberg, C. P., Tada, M., Rauch, G. J., Saude, L., Concha, M. L., Geisler, R., Stemple, D. L., Smith, J. C. and Wilson, S. W. (2000). Silberblick/Wnt11 mediates convergent extension movements during zebrafish gastrulation. *Nature* **405**, 76-81.
Jacobson, A. G. and Gordon, R. (1976). Changes in the shape of the developing vertebrate nervous system analyzed experimentally, mathematically, and by computer simulation. *J. Exp. Zool.* **197**, 191-246.
Jessen, J. R., Topczewski, J., Bingham, S., Sepich, D. S., Marlow, F., Chandrasekhar, A. and Solnica-Krezel, L. (2002). Zebrafish trilobite identifies new roles for Strabismus in gastrulation and neuronal movements. *Nat. Cell Biol.* **4**, 610-615.
Johansen, K. A., Iwaki, D. D. and Lengyel, J. A. (2002). Localized JAK/STAT signaling is required for oriented cell rearrangement in a tubular epithelium. *Development* **130**, 135-145.
Keller, R. (2002). Shaping the vertebrate body plan by polarized embryonic cell movements. *Science* **298**, 1950-1954.
Keller, R. and Danilchik, M. (1988). Regional expression, pattern and timing of convergence and extension during gastrulation of *Xenopus laevis*. *Development* **103**, 193-209.
Keller, R. and Tibbetts, P. (1989). Mediolateral cell intercalation in the dorsal, axial mesoderm of Xenopus laevis. *Dev. Biol.* **131**, 539-549.
Keller, R. and Shook, D. (2008). Dynamic determinations: patterning the cell behaviours that close the amphibian blastopore. *Philos. Trans. R. Soc. Lond. B Biol. Sci.* **363**, 1317-1332.
Keller, R., Shih, J. and Sater, A. (1992a). The cellular basis of the convergence and extension of the *Xenopus* neural plate. *Dev. Dyn.* **193**, 199-217.
Keller, R., Shih, J. and Domingo, C. (1992b). The patterning and functioning of protrusive activity during convergence and extension of the Xenopus organizer. *Dev. Suppl.* 81-91.
Keller, R., Davidson, L., Edlund, A., Elul, T., Ezin, M., Shook, D. and Skoglund, P. (2000). Mechanisms of convergence and extension by cell intercalation. *Philos. Trans. R. Soc. Lond. B Biol. Sci.* **355**, 897-922.
Keller, R., Shook, D. and Skoglund, P. (2008). The forces that shape embryos: physical aspects of convergent extension by cell intercalation. *Phys. Biol.* **5**, 15007.
Keller, R. E. (1981). An experimental analysis of the role of bottle cells and the deep marginal zone in gastrulation of *Xenopus laevis*. *J. Exp. Zool.* **216**, 81-101.
Keller, R. E. (1984). The cellular basis of gastrulation in Xenopus laevis: active, postinvolution convergence and extension by mediolateral interdigitation. *Am. Zool.* **24**, 589-603.
Kibar, Z., Vogan, K. J., Groulx, N., Justice, M. J., Underhill, D. A. and Gros, P. (2001). Ltap, a mammalian homolog of Drosophila Strabismus/Van Gogh, is altered in the mouse neural tube mutant Loop-tail. *Nat. Genet.* **28**, 251-255.
Kibar, Z., Torban, E., McDearmid, J. R., Reynolds, A., Berghout, J., Mathieu, M., Kirillova, I., De Marco, P., Merello, E., Hayes, J. M. et al. (2007). Mutations in VANGL1 associated with neural-tube defects. *N. Engl. J. Med.* **356**, 1432-1437.
Kimmel, C. B., Warga, R. M. and Kane, D. A. (1994). Cell cycles and clonal strings during formation of the zebrafish central nervous system. *Development* **120**, 265-276.
Kinder, S. J., Tsang, T. E., Quinlan, G. A., Hadjantonakis, A. K., Nagy, A. and Tam, P. P. (1999). The orderly allocation of mesodermal cells to the extraembryonic structures and the anteroposterior axis during gastrulation of the mouse embryo. *Development* **126**, 4691-4701.
Lengyel, J. A. and Iwaki, D. D. (2002). It takes guts: the Drosophila hindgut as a model system for organogenesis. *Dev. Biol.* **243**, 1-19.
Lin, F., Sepich, D. S., Chen, S., Topczewski, J., Yin, C., Solnica-Krezel, L. and Hamm, H. (2005). Essential roles of G{alpha}12/13 signaling in distinct cell behaviors driving zebrafish convergence and extension gastrulation movements. *J. Cell Biol.* **169**, 777-787.
Lu, X., Borchers, A. G., Jolicoeur, C., Rayburn, H., Baker, J. C. and Tessier-Lavigne, M. (2004). PTK7/CCK-4 is a novel regulator of planar cell polarity in vertebrates. *Nature* **430**, 93-98.
Martin, P. M. and Sutherland, A. E. (2001). Exogenous amino acids regulate trophectoderm differentiation in the mouse blastocyst through an mTOR-dependent pathway. *Dev. Biol.* **240**, 182-193.
Mlodzik, M. (2002). Planar cell polarization: do the same mechanisms regulate Drosophila tissue polarity and vertebrate gastrulation? *Trends Genet.* **18**, 564-571.
Montcouquiol, M., Rachel, R. A., Lanford, P. J., Copeland, N. G., Jenkins, N. A. and Kelley, M. W. (2003). Identification of Vangl2 and Scrb1 as planar polarity genes in mammals. *Nature* **423**, 173-177.
Moon, R. T., Campbell, R. M., Christian, J. L., McGrew, L. L., Shih, J. and Fraser, S. (1993). Xwnt-5A: a maternal Wnt that affects morphogenetic movements after overexpression in embryos of Xenopus laevis. *Development* **119**, 97-111.
Murdoch, J. N., Doudney, K., Paternotte, C., Copp, A. J. and Stanier, P. (2001). Severe neural tube defects in the loop-tail mouse result from mutation of Lpp1, a novel gene involved in floor plate specification. *Hum. Mol. Genet.* **10**, 2593-2601.
Myers, D. C., Sepich, D. S. and Solnica-Krezel, L. (2002). Convergence and extension in vertebrate gastrulae: cell movements according to or in search of identity? *Trends Genet.* **18**, 447-455.
Schechtman, A. M. (1942). The mechanism of amphibian gastrulation. I. Gastrulation-promoting interactions between various regions of ananural egg. (*Hyla regilla*). *Univ. Calif. Publ. Zool.* **51**, 1-39.
Schoenwolf, G. C. and Alvarez, I. S. (1989). Roles of neuroepithelial cell rearrangement and division in shaping of the avian neural plate. *Development* **106**, 427-439.
Schoenwolf, G. C. and Alvarez, I. S. (1992). Role of cell rearrangement in axial morphogenesis. *Curr. Top. Dev. Biol.* **27**, 129-173.
Sepich, D. S., Myers, D. C., Short, R., Topczewski, J., Marlow, F. and Solnica-Krezel, L. (2000). Role of the zebrafish trilobite locus in gastrulation movements of convergence and extension. *Genesis* **27**, 159-173.
Sepich, D. S., Calmelet, C., Kiskowski, M. and Solnica-Krezel, L. (2005). Initiation of convergence and extension movements of lateral mesoderm during zebrafish gastrulation. *Dev. Dyn.* **234**, 279-292.
Shih, J. and Keller, R. (1992a). Cell motility driving mediolateral intercalation in explants of *Xenopus laevis*. *Development* **116**, 901-914.
Shih, J. and Keller, R. (1992b). Patterns of cell motility in the organizer and dorsal mesoderm of *Xenopus laevis*. *Development* **116**, 915-930.
Shnitsar, I. and Borchers, A. (2008). PTK7 recruits dsh to regulate neural crest migration. *Development* **135**, 4015-4024.
Smith, J. C., Conlon, F. L., Saka, Y. and Tada, M. (2000). Xwnt11 and the regulation of gastrulation in Xenopus. *Philos. Trans. R. Soc. Lond. B Biol. Sci.* **355**, 923-930.
Smith, J. L., Gesteland, K. M. and Schoenwolf, G. C. (1994). Prospective fate map of the mouse primitive streak at 7.5 days of gestation. *Dev. Dyn.* **201**, 279-289.
Stephens, L. E., Sutherland, A. E., Klimanskaya, I. V., Andrieux, A., Meneses, J., Pedersen, R. A. and Damsky, C. H. (1995). Deletion of beta 1 integrins in mice results in inner cell mass failure and peri-implantation lethality. *Genes Dev.* **9**, 1883-1895.
Sulik, K., Dehart, D. B., Iangaki, T., Carson, J. L., Vrablic, T., Gesteland, K. and Schoenwolf, G. C. (1994). Morphogenesis of the murine node and notochordal plate. *Dev. Dyn.* **201**, 260-278.
Tada, M. and Smith, J. C. (2000). Xwnt11 is a target of Xenopus Brachyury: regulation of gastrulation movements via Dishevelled, but not through the canonical Wnt pathway. *Development* **127**, 2227-2238.
Tada, M., Concha, M. L. and Heisenberg, C. P. (2002). Non-canonical Wnt signalling and regulation of gastrulation movements. *Semin. Cell Dev. Biol.* **13**, 251-260.
Torban, E., Patenaude, A. M., Leclerc, S., Rakowiecki, S., Gauthier, S., Andelfinger, G., Epstein, D. J. and Gros, P. (2008). Genetic interaction between members of the Vangl family causes neural tube defects in mice. *Proc. Natl. Acad. Sci. USA* **105**, 3449-3454.
Trinkaus, J. P. (1998). Gradient in convergent cell movement during Fundulus gastrulation. *J. Exp. Zool.* **281**, 328-335.
Veeman, M. T., Slusarski, D. C., Kaykas, A., Louie, S. H. and Moon, R. T. (2003). Zebrafish prickle, a modulator of noncanonical wnt/fz signaling, regulates gastrulation movements. *Curr. Biol.* **13**, 680-685.
Voiculescu, O., Bertocchini, F., Wolpert, L., Keller, R. E. and Stern, C. D. (2007). The amniote primitive streak is defined by epithelial cell intercalation before gastrulation. *Nature* **449**, 1049-1052.
Wallingford, J. B. and Harland, R. M. (2001). Xenopus Dishevelled signaling regulates both neural and mesodermal convergent extension: parallel forces elongating the body axis. *Development* **128**, 2581-2592.
Wallingford, J. B. and Harland, R. M. (2002). Neural tube closure requires Dishevelled-dependent convergent extension of the midline. *Development* **129**, 5815-5825.
Wallingford, J. B., Rowning, B. A., Vogeli, K. M., Rothbacher, U., Fraser, S. E. and Harland, R. M. (2000). Dishevelled controls cell polarity during Xenopus gastrulation. *Nature* **405**, 81-85.
Wang, J., Hamblet, N. S., Mark, S., Dickinson, M. E., Brinkman, B. C., Segil, N., Fraser, S. E., Chen, P., Wallingford, J. B. and Wynshaw-Boris, A. (2006). Dishevelled genes mediate a conserved mammalian PCP pathway to regulate convergent extension during neurulation. *Development* **133**, 1767-1778.
Wilson, P. and Keller, R. (1991). Cell rearrangement during gastrulation of Xenopus: direct observation of cultured explants. *Development* **112**, 289-300.
Wilson, P. A., Oster, G. and Keller, R. (1989). Cell rearrangement and segmentation in Xenopus: direct observation of cultured explants. *Development* **105**, 155-166.

Yang, X., Dormann, D., Munsterberg, A. E. and Weijer, C. J. (2002). Cell movement patterns during gastrulation in the chick are controlled by positive and negative chemotaxis mediated by FGF4 and FGF8. *Dev. Cell* **3**, 425-437.
Ybot-Gonzalez, P., Savery, D., Gerrelli, D., Signore, M., Mitchell, C. E., Faux, C. H., Greene, N. D. and Copp, A. J. (2007). Convergent extension, planar-cell-polarity signalling and initiation of mouse neural tube closure. *Development* **134**, 789-799.
Yin, C., Kiskowski, M., Pouille, P. A., Farge, E. and Solnica-Krezel, L. (2008). Cooperation of polarized cell intercalations drives convergence and extension of presomitic mesoderm during zebrafish gastrulation. *J. Cell Biol.* **180**, 221-232.
Zallen, J. and Wieschaus, E. (2004). Patterned gene expression directs bipolar planar polarity in Drosophila. *Dev. Cell* **6**, 343-355.
Zar, J. H. (1998). *Biostatistical Analysis*. Upper Saddle River, NJ: Prentice-Hall.